First-principles investigation of structural and electronic properties of solid cubane and its doped derivatives

T. Yildirim
NIST Center for Neutron Research, Gaithersburg, Maryland 20899

S. Ciraci, Ç. Kılıç, and A. Buldum*
Department of Physics, Bilkent University, Ankara, Turkey

(Received 17 December 1999; revised manuscript received 8 May 2000)

The electronic and structural properties of molecular and solid cubane have been studied by first-principles, self-consistent field total energy calculations. Calculated molecular properties such as equilibrium geometry and electronic and vibrational spectra are found to be in good agreement with experimental data. Structural parameters and the energetics of both the low-temperature, orientationally ordered and high-temperature, orientationally disordered or plastic phases of solid cubane are determined. The valence band of solid cubane is derived from the molecular states; the energy gap between the lowest unoccupied and highest occupied molecular orbital bands is rather large due to the saturated carbon atoms. The effect of alkali-metal-atom doping on the electronic energy bands is investigated. It is found that the metallic band of doped cubane is derived from the undoped solid cubane's lowest conduction band with a significant contribution from the alkali-metal atom.

I. INTRODUCTION

Cubane (C_8H_8) has one of the most interesting and unusual structures among all carbon molecules; it is an atomic scale realization of a cube with eight carbon atoms arranged at the corners and single hydrogen atoms bonded to each carbon atom along the body diagonals (see Fig. 1).[1,2] Accordingly, the C-C-C bond angle is 90°, rather than the 109.5° normally found in the tetrahedral sp^3 bonding of group IV elements. This structure results in a significant amount of strain energy, roughly 6.5 eV per molecule,[3] so that the transitions to other more stable molecules are extremely exothermic. Because of its high heat of formation and high density, the cubane molecule and its derivatives are candidates for highly energetic materials and fuels.[4] Since the first synthesis by Eaton and Cole,[1,2] cubane has been a subject of active research. The cubic structure has been confirmed using a variety of experimental techniques including infrared and Raman spectroscopy,[5–7] high-resolution laser spectroscopy,[8] and x-ray diffraction.[9] A number of theoretical studies performed at both the semiempirical and *ab initio* levels have clarified the electronic states of the molecule.[10–15]

In 1964 Fleischer[9] showed that cubane forms a stable solid at room temperature with a crystalline structure composed of cubane molecules occupying corners of the rhombohedral primitive unit cell (space group $R\bar{3}$). The cubic molecular geometry gives the solid many unusual electronic,[16] structural, and dynamical[16–19] properties compared to the other hydrocarbons. For example, solid cubane has a relatively high melting point temperature (405 K) and a very high frequency for the lowest-lying intramolecular vibrational mode ($617\ \mathrm{cm}^{-1}$).[5,6,14] Recent work related to cubane has focused on solid cubane and cubane based derivatives.[17–24] Because of relatively weak intermolecular interaction the cohesive energy relative to the constituent C_8H_8 is expected to be small, and most of the physical properties of solid cubane are dominated by the properties of the C_8H_8 molecule.

Solid cubane undergoes a first-order phase transition at $T_c = 394$ K from an orientationally ordered phase to a noncubic orientationally disordered (plastic) phase, resulting in a significant volume expansion of 5.4%.[20] Despite many studies, including Raman spectroscopy,[6] adiabatic and differential-scanning calorimetry,[18] and NMR studies,[18,19] which all show evidence for such a transition, the structure of the high-temperature phase was only recently identified.[20] It was found that this phase is also rhombohedral and has the rhombohedral angle $\alpha = 103.3°$. The plastic phase persists until $T = 405$ K, at which point cubane melts. The tempera-

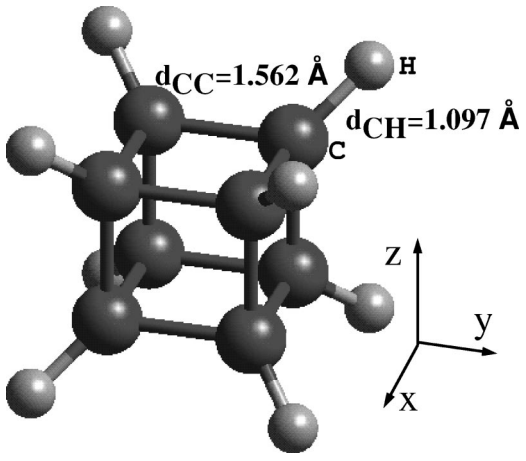

FIG. 1. Cubane molecule in its standard orientation. Dark large spheres represent carbon atoms, while small gray spheres represent hydrogen atoms. The cubic structure is uniquely characterized by two bond lengths, d_{CC} and d_{CH}.

ture dependence of the properties of solid cubane is also very interesting.[20] It shows a very large thermal expansion and model calculations indicate very large amplitude orientational dynamics.[20]

In this paper, we investigate the structural, dynamical, and electronic properties of the cubane molecule and solid cubane. Our objective is to present a systematic analysis of these properties based on first-principles self-consistent field (SCF) calculations within the local density approximation (LDA). In order to guide future experimental work on cubane, we also explore the doping of solid cubane with alkali-metal atoms and examine how the electronic states and charge density are modified upon doping. This paper is organized as follows. In the next section, we discuss the computational method. In Sec. III, we present the results of our calculations obtained for the electronic energy, structure, and vibrational frequencies of an isolated cubane molecule. In Sec. IV, we investigate the structural properties of solid cubane. In Sec. V, we concentrate on the electronic properties of solid cubane. We calculate the electronic energy, band structure, and total density of electronic states (DOS) for the low-temperature phase with the optimized structure. In Sec. VI, we examine the electronic and structural properties of the alkali-metal-atom doped derivative of solid cubane. Finally, our conclusions are summarized in Sec. VII.

II. COMPUTATIONAL METHOD

Structural, electronic, and dynamic properties of the cubane molecule and solid cubane have been calculated using the SCF pseudopotential method in momentum space within the LDA. We used optimized, nonlocal, norm-conserving ionic pseudopotentials in the Kleinman-Bylander form[26] and the Ceperly-Alder exchange-correlation potential[27] in the form parametrized by Perdew and Zunger.[28] While calculating alkali-metal doping we took the core corrections to the potassium pseudopotential into account. In the plane wave calculations the software package CASTEP (Refs. 29, 30) has been used. Further details of the *first-principles* method can be obtained in Ref. 30. The electronic wave functions are represented by plane waves with cutoff energy of 1500 eV. For molecular calculations within the supercell approach the Brillouin zone integration has been performed using only the $\mathbf{k}=\mathbf{0}$ point, which is sufficient due to the large size of the cell and also because the lowest unoccupied molecular orbital (LUMO) state is well separated from the highest occupied molecular orbital (HOMO) state. For the calculation of solid cubane we used 38 $\mathbf{k}$ points in the irreducible Brillouin zone determined according to the Monkhorst and Pack[31] scheme. In all calculations, a finite basis correction[30] with cutoff energy [i.e., $dE/d\ln(E_{\text{cutoff}})$] was calculated and found to be less than -0.05 eV/atom, confirming the convergence of the calculations. Structural optimizations were performed by using the BFGS minimization technique.[32] In order to determine if the supercell method is suitable for calculating the physical properties of an isolated molecule in momentum space, we also performed a SCF electronic structure calculation of C_8H_8 using a local basis set expressed in terms of Gaussian type orbitals.[29,33]

III. ELECTRONIC AND VIBRATIONAL PROPERTIES OF THE CUBANE MOLECULE

We study the electronic structure of an isolated cubane molecule by treating the molecular orbitals in terms of local Gaussian orbitals. We also investigate the electronic and vibrational properties of the molecule by using the supercell approach. The supercell is constructed by placing the cubane molecules in a simple cubic lattice with the lattice constant $a_s=16$ Å, which is periodically repeated in three dimensions. Owing to the large distance between adjacent cubane molecules (approximately three times larger than the lattice constant of solid cubane) the intermolecular interactions are negligible and the results that we obtained can be attributed to an isolated cubane molecule. By comparing the results obtained from the two approaches we test the accuracy of the plane wave basis set for further calculations on the molecular crystal.

The C-C bond length d_{CC} and C-H bond length d_{CH} are determined by optimizing the structure within $P1$ symmetry. The full optimization of the structure is achieved by reducing the force on each atom to a value less than 0.005 eV/Å. The optimized structure has cubic symmetry with bond lengths $d_{\text{CC}}=1.551$ Å and $d_{\text{CH}}=1.098$ Å, in good agreement with experimental data ($d_{\text{CC}}=1.562$ Å and $d_{\text{CH}}=1.097$ Å).[34] The electronic energy structure calculated with the local basis set and supercell methods is presented together with the symmetry assignments in Fig. 2(a). After aligning the HOMO energies, the maximum deviation between the energy states is seen to be less than 0.1 eV. The energies of the filled states are grouped in five regions, each separated by large gaps. Such large gaps result from the strained cubic structure of the molecule. The gap between the HOMO and LUMO $E_{g,LH}$ is large (6.9 eV) owing to the saturation of the carbon atoms. The calculated value of $E_{g,LH}$ depends on how the exchange-correlation potential is treated. Calculations based on the LDA usually underestimate the gap energy. In fact, restricted Hartree-Fock calculations[15] yield $E_{g,LH}=15.48$ eV. The energy gap predicted by calculations based on density functional theory (DFT) with the B3LYP exchange-correlation potential[35] is 8.6 eV, which seems to be a reasonable value.[15] Nevertheless, $E_{g,LH}$ is expected to be larger than the value predicted by the LDA calculations.

Recently, the vibrational spectrum of cubane has been studied by using neutron scattering and a detailed comparison has been made with various theories from phenomenological tight-binding to a first-principles calculation with a local basis such as a Gaussian.[14] Here we calculate the NIS (neutron inelastic scattering) spectrum[36] and compare it with experimental data[14] to further establish the accuracy of the plane wave technique in such a strained molecular system. The vibrational modes and their frequencies are obtained by the direct force method using the supercell geometry.

The cubane molecule has 42 internal degrees of freedom and thus has 42 vibrational modes. Because of the highly symmetric structure of C_8H_8 these eigenmodes have only 18 distinct frequencies, i.e., $2\times(2A+5T+2E)$. The vibrational mode energies of cubane obtained from supercell calculation and from Raman and infrared experiments (in parentheses) are shown in Fig. 2(b). The agreement between the calculation and the experimental data[5,7,14] is quite good. Clearly, the

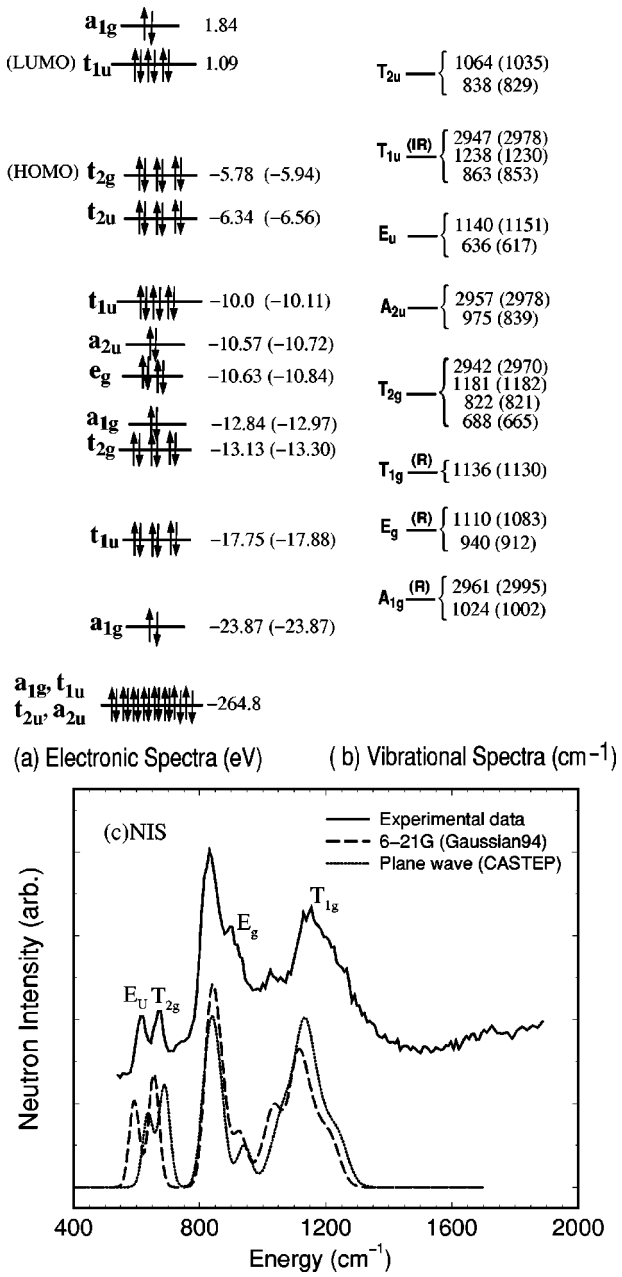

FIG. 2. Electronic and vibrational spectra of the cubane molecule. (a) Molecular orbital energies. Numbers in parentheses are from *ab initio* calculations using the plane wave basis set, while other numbers are from the Gaussian basis (Refs. 14,15). (b) Vibrational spectra. (R) and (IR) indicate Raman- and infrared-active modes, respectively. Experimental data for vibrational spectrum (Refs. 5,7,14) are indicated in parentheses. (c) Neutron inelastic spectrum of cubane vibration is compared to that obtained from the plane wave calculation. For comparison we also show the spectrum calculated using the 6-21 Gaussian basis (Ref. 14).

supercell calculation with plane wave basis provides vibrational frequencies as accurate as those obtained by using methods that employ a Gaussian basis.[14] In spite of the fact that the cubane structure is highly strained, the vibrational modes involving C-H stretching, i.e., A_2u, T_2g, T_1u, and A_1g at ~ 3000 cm^{-1}, are very similar to those in unstrained hydrocarbons. However, the overall mode energies (particularly those involving C-C stretching, i.e., T_2g, T_2u, T_1u, E_g, and A_1g modes ranging from 822 cm^{-1} to 1024 cm^{-1}) are rather high and reflect the highly strained structure of the cubic cage. As seen in Fig. 2(b), the calculated vibrational energies are in almost perfect agreement with the Raman and infrared data (shown in parentheses). The most significant deviation is for the A_{2u} mode, which is calculated to be 975 cm^{-1}, while the experimental value is 839 cm^{-1}. Interestingly, the same disagreement exists in the calculations using the Gaussian basis,[14] indicating a possible error in the assignment of the modes from the experimental data. A more stringent test for the present calculations is to actually compare the intensities of the vibrational modes (which involve eigenvectors), rather than the frequencies of the modes. NIS is the perfect tool for that purpose. Details of the neutron inelastic scattering measurements of the vibrational spectrum were given elsewhere.[14] Here we compare only the calculated NIS spectrum with the experimental data as shown in Fig. 2(c). The calculated NIS spectrum reproduces all the features at the correct energies observed in the experiment. An important conclusion drawn from this section is that the supercell calculation with plane wave basis set is very successful in predicting many molecular properties, from bond lengths to vibrational spectrum intensities. In the rest of the paper, we will investigate the solid state properties of cubane and its hypothetical alkali-metal-doped derivatives by using SCF pseudopotential calculations in momentum space within the LDA.

IV. STRUCTURAL PROPERTIES OF SOLID CUBANE

Both the ordered and disordered phases of solid cubane have a rhombohedral lattice with space group $R\bar{3}$. The structure can be characterized by three parameters: the lattice constant a, the rhombohedral angle α, and the setting angle ϕ (i.e., the orientation of the cubane molecule). The unit cell can be viewed as a fcc lattice that has been squashed along a particular axis that remains the threefold axis of the crystal. In this way α increases from the fcc value of 60° to 72.7°, but it is still significantly smaller than the rhombohedral angle of the bcc structure where $\alpha = 109.47°$. The crystal structure with one C_8H_8 molecule per unit cell together with the lattice parameters, and also the view along the threefold rhombohedral axis are shown in Fig. 3. The setting angle of the cubane molecule, i.e., the rotation of the molecule about the threefold axis, is not fixed by the symmetry, and therefore can take any value. Experimentally, the setting angle is determined to be 46°.[9,20] This orientation brings the hydrogen atoms of one molecule into close proximity with the midpoints of the C-C bonds of the neighboring molecules. This alignment is perfect when $\phi = 45.57°$.

We first perform a full structure optimization of both lattice parameters (a and α) and atomic positions (which also sets ϕ) by using BFGS minimization[32] within the constraint of rhombohedral symmetry. The very rigid cubic skeleton of the molecule is slightly distorted due to the weak crystal field of the nearest neighbor molecules, yielding C-H distances of 1.100 Å (along the [111] axis) and 1.101 Å (for other directions). Similarly, C-C bond distances are about 1.558 Å and the C-C-C angles change from 89.9° to 90.0°, reflecting a tiny distortion away from cubic symmetry. The optimized values of a, α, and ϕ are $a_0 = 5.07$ Å, $\alpha_1 = 71.34°$, and ϕ

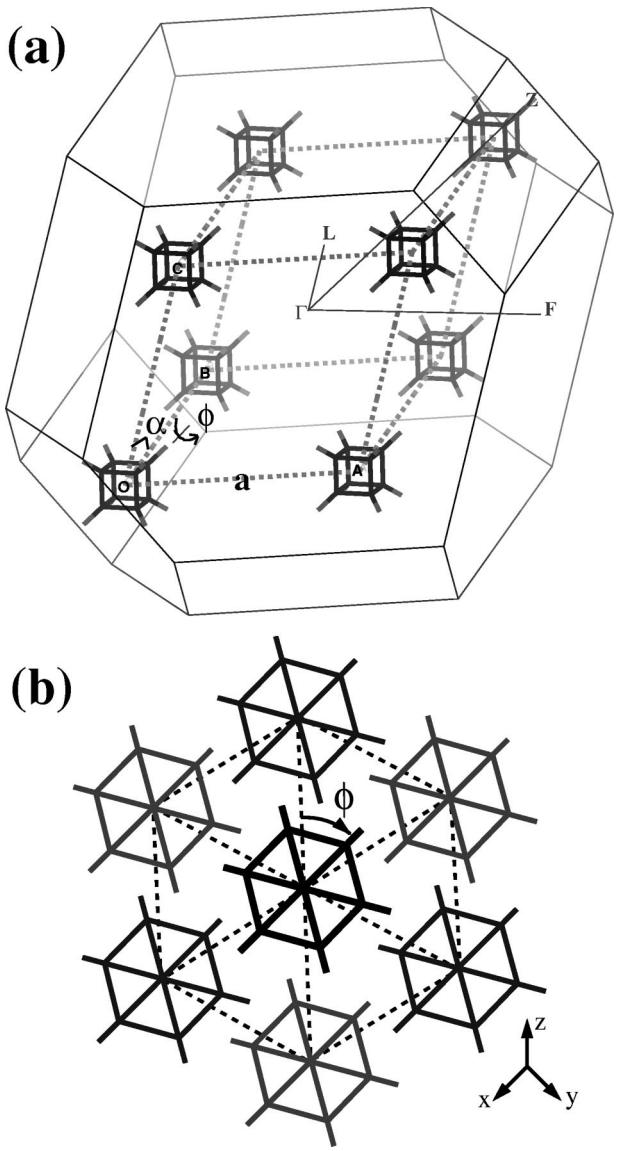

FIG. 3. (a) A schematic representation of the rhombohedral unit cell of solid cubane in the ordered phase. The corresponding first Brillouin zone together with symmetry directions (Γ-L,Γ-Z,Γ-F) are also shown. The lattice parameter a, the rhombohedral angle α, and the setting angle of the cubane molecules, ϕ, are indicated. (b) A view of the unit cell along the threefold [111] axis of the rhombohedral cell.

$=45°$, respectively, in good agreement with the experimental data at 77 K;[20] $a_{\mathrm{exp}}=5.20$ Å, $\alpha_{\mathrm{exp}}=72.7°$, and $\phi_{\mathrm{exp}}=46°$.

Next we examine the variation of the total energy $E_T(\mathrm{s\text{-}C_8H_8})$ as a function of only one parameter while keeping the other two parameters fixed at their optimized values. Figure 4(a) illustrates the variation of the total energy E_T with the lattice constant a. The cohesive energy is calculated as the difference between the total energy of the isolated cubane molecule and the total energy of the solid cubane:

$$E_{coh}=E_T(\mathrm{C_8H_8})-E_T(\mathrm{s\text{-}C_8H_8}). \tag{1}$$

According to this definition $E_{coh}>0$ indicates the stable binding state. We calculated $E_{coh}=680$ meV per C_8H_8 molecule at the optimized lattice parameter $a_0=5.07$ Å.

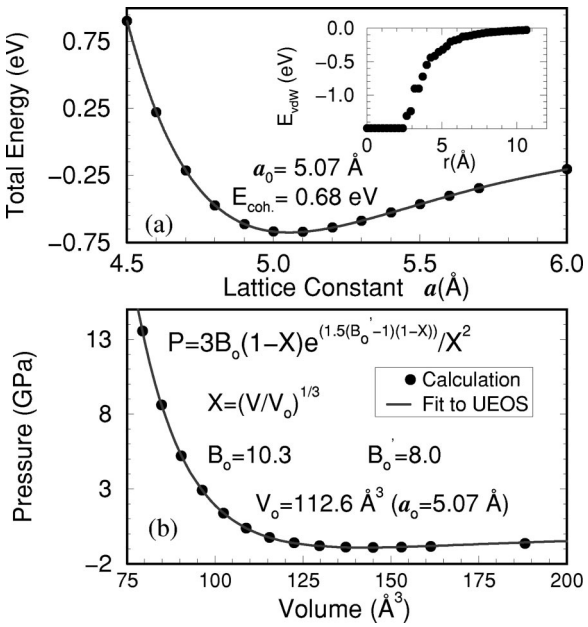

FIG. 4. (a) Total energy E_T of solid cubane as a function of lattice parameter a in the ordered phase (i.e., $\alpha=71.34°$). The zero of energy is taken as the total energy of the C_8H_8 molecule calculated by the supercell method. The equilibrium value of the lattice constant a and the cohesive energy E_{coh} are also given. The inset shows the van der Waals interaction ($E_{vdW}=-\Sigma_{r_{ij}\leq r_c}C_{ij}/r_{ij}^6$) as a function of cutoff distance (r_c). The coefficients C_{ij} are estimated from the Slater-Kirkwood approximation (Ref. 46). (b) Pressure versus lattice constant curve for solid cubane in its low-temperature, orientationally ordered phase. The solid line is a fit based on the universal equation of state given in the figure (Ref. 47).

We make the following comments related to the cohesive energy: (i) The calculated cohesive energy in Eq. (1) comprises only the short-range interaction, and is obtained from minimization of the expectation value of the electronic Hamiltonian and the Coulombic ion-ion interaction.[30] It is weak as compared to the cohesive energy of many metals and semiconductors due to the weak intermolecular interaction, which results in a weak polarization of the charge of isolated molecules. On the other hand, it is much larger than that obtained from purely van der Waals (vdW) interactions,[37–41] which is estimated to be around -0.25 eV, as shown in the inset to Fig. 4. (ii) It is usually asserted that inert gas and molecular crystals are bound by the vdW interaction,[25,26] which is not taken into account by DFT. In contrast to this argument, the present LDA calculation is able to predict the lattice constant of solid cubane in good agreement with experimental value. Interestingly, similar calculations carried out within the generalized gradient approximation predicted a much larger lattice constant ($a=6$ Å) and a very small cohesive energy ($E_{coh}=110$ meV).[42] In the past, similar paradoxical situations occurred for the physisorption of Xe on metal surfaces. It was usually argued that the charge rearrangement upon physisorption of closed-shell atoms is negligible and hence does not include any short-range attractive interaction. Lang,[43] on the other hand, provided a good account of experimental data on atomic binding energy within DFT. His results are confirmed by work function measurements[44] and SCF pseudopotential calculations.[45]

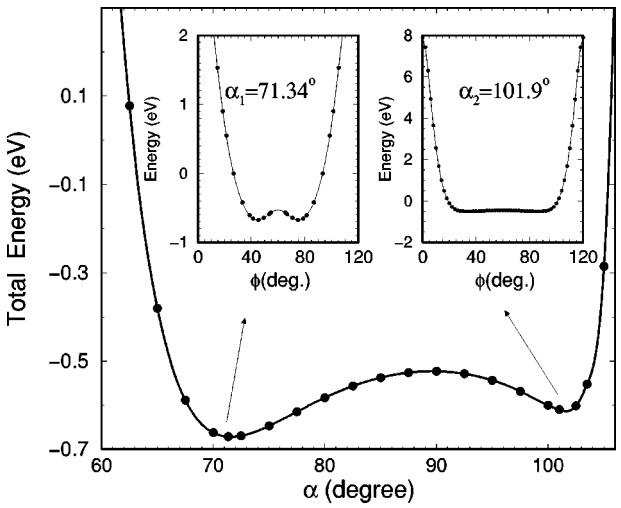

FIG. 5. Variation of the total energy as a function of the rhombohedral angle α. The global and local minima at $\alpha_1=71.34°$ and $\alpha_2=101.9°$ are in good agreement with the experimental values of $\alpha_1=72.6°$ and $\alpha_2=103.3°$. The insets show the variation of the total energy as all the cubane molecules rotate about the principal ([111]) axis of the rhombohedron (defined as setting angle ϕ) in the global (i.e., $\alpha=\alpha_1$) and local (i.e., $\alpha=\alpha_2$) minima.

In Fig. 4(b), we show the variation of the hydrostatic pressure with volume. In the same figure the fit to the *universal equation of the state*,[47] i.e., $P(V/V_0)$ where V_0 is the equilibrium volume with $a=a_0$, is shown. Using this fit, one obtains the bulk modulus $B=-Vdp/dV$ as 10.3 GPa. This value is about half of that for molecular solid C_{60},[48] suggesting that cubane is twice softer than solid C_{60}. However, the pressure derivative of the bulk modulus B_o' calculated here is about the same as that for solid C_{60}.[48] It will be interesting to compare these results to experimental data for solid cubane when it is available.

The variation of the total energy with the rhombohedral angle α is illustrated in Fig. 5, where the lattice constant a and the setting angle ϕ are kept at their optimized values. We note that $E_T(\alpha)$ has two minima. The first one is the global minimum at $\alpha_1=71.34°$ that corresponds to the low-temperature, orientationally ordered phase. The second minimum at $\alpha_2=101.9°$ is only a local minimum and hence it occurs at higher energy. It corresponds to the high-temperature, orientationally disordered phase ($\alpha_{\rm exp}=103.3°$). The energy barrier ΔE for order-disorder structural transformation is estimated from Fig. 5 to be ~ 150 meV at $T=0$. It is shown that such a transition occurs at $T_c=394$ K followed by a sudden increase of the lattice parameter ($\Delta a/a=1\%$) and the rhombohedral angle ($\alpha_1 \rightarrow \alpha_2$, i.e., $\Delta\alpha \sim 30.6°$), which corresponds to a volume change of $\Delta V/V=5.4\%$.[20]

Next we investigate the variation of the total energy E_T with the third structural parameter ϕ at these two minima at $\alpha=\alpha_1$ and $\alpha=\alpha_2$. The results of our *ab initio* calculations are shown as insets in Fig. 5. The left inset corresponds to the curve $E_T(a=a_0,\alpha=\alpha_1,\phi)$, and exhibits two distinct minima at $\phi_1=45°$ and at its symmetry equivalent value, $\phi_2=2\pi/3-\phi_1$. The results of our *ab initio* calculations are in good agreement with the experimentally determined value $\phi_{\rm exp}=46^{\rm o}$. From the curvature of $E_T(a=a_0,\alpha=\alpha_1,\phi)$ at $\phi=\phi_1$ we estimate the frequency of the A_g libration mode at $T=0$ K to be 136 $\rm cm^{-1}$, which is in fair agreement with the experimental value of 115 $\rm cm^{-1}$ measured using neutron inelastic scattering methods (at 100 K).[17] The curve $E_T(a=a_0,\alpha=\alpha_2,\phi)$ presented in the right inset shows the orientational dependence of the potential for the high-T phase (i.e., $\alpha=\alpha_2$); it is almost flat for a wide range of setting angle $25°<\phi<95°$. This implies that for the high-temperature phase E_T is nearly independent of ϕ, and hence the orientation of cubane molecule cannot be fixed in this range. This situation is a good example of a system with collective large amplitude motions. It is suggested that the softening of the librational modes is the driving mechanism for the observed order-disorder structural transformation.[20] Another interesting point is that normally the orientational disorder in the plastic phase tends to average out the molecular symmetry, making it more spherical. Therefore, a close-packed fcc structure is expected to occur as a result of the order-disorder phase transition. Contrary to this expectation, the high-temperature disordered (or plastic phase) of solid cubane is neither cubic nor close packed; it is rhombohedral with $\alpha=103.3°$.[20] In this respect solid cubane is an unusual example.

In concluding this section, first-principles calculations presented here are successful in predicting the structural properties of solid cubane. Richardson and Martins[24] have recently reported similar *ab initio* calculations by using soft pseudopotentials.[49] However, they concluded that the LDA did not work well for solid cubane, in contrast to our results. In their work, the setting angle of the cubane molecule (ϕ) in the structure was not mentioned at all. It was stated that the rhombohedral crystal structure of solid cubane is uniquely characterized by a and α. As revealed from the above discussion, this statement is clearly incomplete and there is a third important parameter, which is the setting angle of the cubane molecule (ϕ). The total energy of the system and the lattice parameter are very sensitive to this parameter as shown in Fig. 5. This could be one of the reasons for the disagreement. In addition to this, they used only two **k** points, which may not be enough for convergence. In the present work, we used 38 **k** points in the irreducible Brillouin zone.

V. ELECTRONIC STRUCTURE OF SOLID CUBANE

The lattice parameters optimized at the global minimum corresponding to the low-temperature, orientationally ordered phase (i.e., $a_0=5.07$ Å, $\alpha_1=71.34°$, and $\phi=45°$) are used for the band calculations. The calculated energy bands are presented in Fig. 6(a). Owing to the weak intermolecular coupling (or small wave function overlap) the dispersion of the valence bands is reminiscent of the bands of other molecular crystals. The dispersion of the valence bands ΔE_{W_D} is within ~ 1 eV. On the other hand, the band dispersion in the range of ~ 1 eV can be taken as an indication of a significant chemical interaction taking part in the cohesion. The electronic structure of solid cubane is derived from the orbital states of the C_8H_8 molecule; the valence band states occur approximately at the same energies, but they exhibit a small dispersion in the first Brillouin zone. Consequently, valence bands are grouped at five energy regions similar to that of the C_8H_8 molecule, where their relative

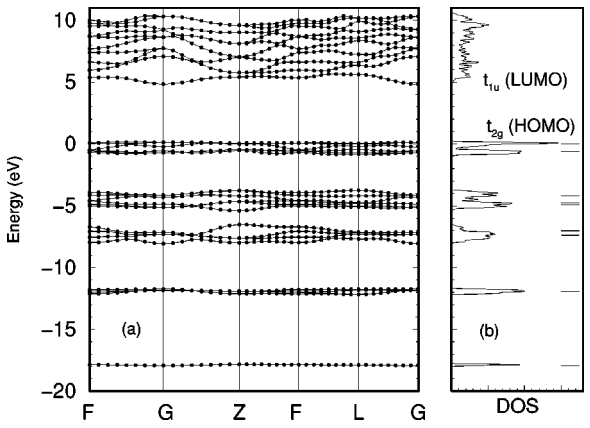

FIG. 6. (a) Energy band structure and (b) electronic total density of states (DOS) of solid cubane in the optimized low-temperature phase, corresponding to $a=5.07$ Å, $\alpha=71.34°$, and $\phi=45°$. Horizontal lines in the right panel mark the orbital energies of an individual cubane molecule. The zero of energy is set at the maximum of the valence bands.

positions are slightly modified. The highest valence band is derived from the t_{2g} orbital (LUMO) state. The bands that are adjacent to the LUMO band originate from the threefold degenerate t_{2u} orbital state. Approximately 3.5 eV below these bands one sees bands derived from t_{1u}, a_{2u}, and e_g orbital states. As the band energy is lowered, the bands become flatter. The bands located around ~8, 12, and 18 eV are derived from the $a_{1g}+t_{2g}$, t_{1u}, and a_{1g} orbital states of the C_8H_8 molecule, respectively.

The conduction bands have relatively large dispersion ($\Delta E_{W_c}\sim 2$ eV) owing to the relatively strong coupling between nearest neighbor antibonding molecular orbitals. The gap between the valence and conduction bands is $E_g \sim 5$ eV at the center of the Brillouin zone (Γ point). We believe that this gap is slightly underestimated by the local density approximation. On the other hand, the gap of 5 eV between the LUMO and HOMO bands is significantly larger than the band gap in fullerenes. This is due to the fact that each carbon atom in the cage of a cubane molecule is connected to three nearest neighbor carbon atoms and also to one hydrogen atom, and hence forms four bonds. In this way the carbon atoms become saturated and E_g is larger than in the case of the fullerenes, which have unsaturated bonds.

The density of electronic states shown in Fig. 6(b), i.e., $\mathcal{D}(E)=\Sigma_{n,\mathbf{k}}\delta(E-E_{n,\mathbf{k}})$, is generated by calculating the band states $E_{n,\mathbf{k}}$ at 180 $\mathbf{k}$ points in the first Brillouin zone, and by broadening them with a Gaussian. One sees that the valence band states of solid cubane are grouped in bands which appear as seven sharp peaks separated by four gaps. The density of electronic states in the high-T phase (i.e., $\alpha=101.9°$) is also calculated and found to be very similar to that in the low-T phase shown in Fig. 6(b). However, we observed significant changes in the DOS with the setting angle ϕ. This is because atoms on different molecules get closer to each other at some particular values of ϕ (for example, $\phi=0$), giving rise to splitting and broadening of the peaks in the DOS. This is also evident from the orientational dependence of the potential energy shown in Fig. 5. Such a strong dependence of the DOS on ϕ may result in interesting coupling between the librons and the electronic structure.

TABLE I. Optimized values of the structural parameters and the corresponding changes in the unit cell volume for AC_8H_8 (A=Li, Na, and K).

	A		
	Li	Na	K
a(Å)	5.63	5.76	5.86
α (deg)	84.0	81.21	77.27
V(Å^3)	175.2	185.0	188.4
$\Delta V/V_0$ (%)	54.6	63.2	66.2

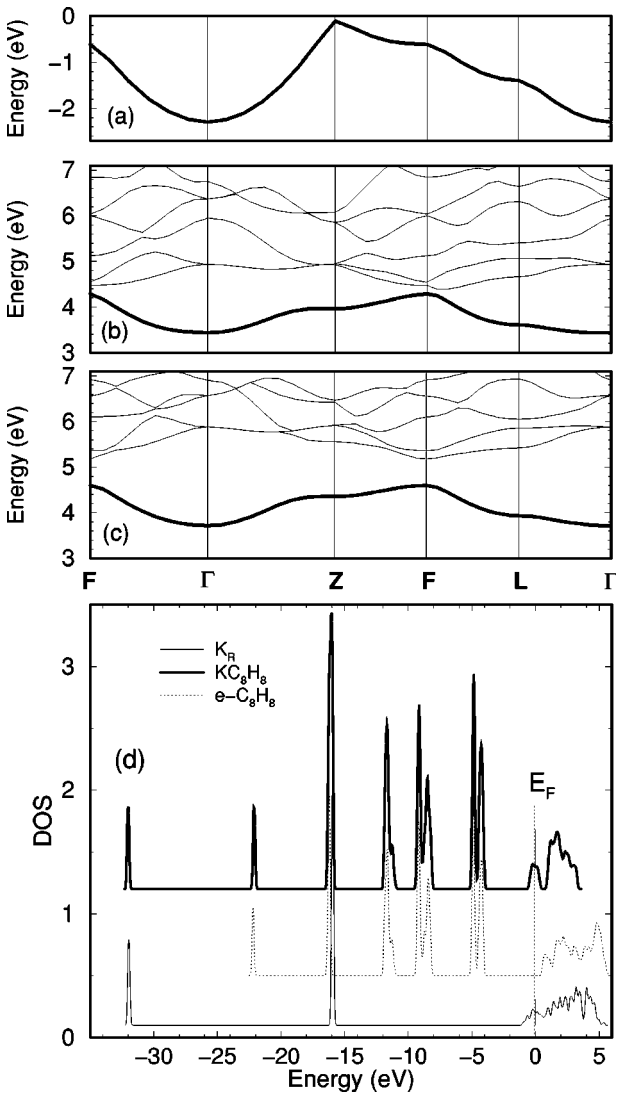

FIG. 7. Conduction band of (a) K_R; (b) e-C_8H_8; (c) KC_8H_8, all having the same lattice parameters as the optimized KC_8H_8. The first conduction bands are illustrated by a thicker line. (d) Total density of electronic states (DOS) calculated for KC_8H_8, e-C_8H_8, and K_R. Zero of energy is taken at the Fermi level E_F of both KC_8H_8 and K_R. The energy of e-C_8H_8 is shifted to align its lowest valence band derived from the molecular a_{1g} state with that of KC_8H_8.

VI. ALKALI-METAL-ATOM DOPED SOLID CUBANE

Solid cubane is a band insulator. Since the conduction bands have relatively small dispersion, they can yield a high

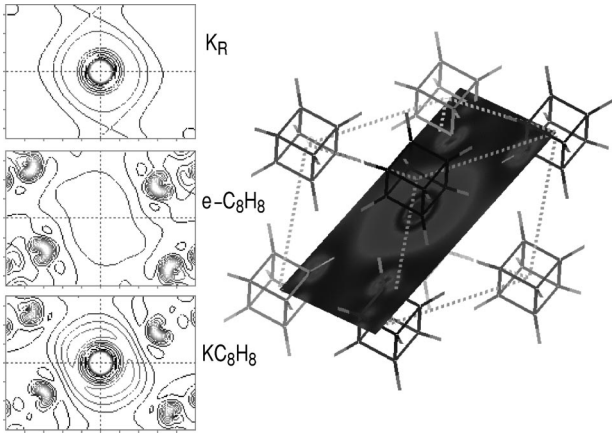

FIG. 8. Contour plots of the charge density for the first conduction band of K_R (top), the lowest conduction band (LUMO) of e-C_8H_8 (middle), and the first conduction band of KC_8H_8 (bottom). Right panel shows the orientation of the contour plane with respect to the lattice.

density of states at the Fermi level E_F when they are occupied. Additional electrons to occupy the empty conduction band can be provided by doping with alkali-metal atoms, since alkali-metal atoms, such as K and Na, can donate their valence electrons to the empty conduction band, as realized, for example, in fullerene intercalation. An interesting aspect here is whether the dopants donate their valence electrons to the conduction (LUMO) band of the crystal, or form a new metallic band in the gap derived from the valence state of the alkali-metal atoms. Modification (or polarization) of the LUMO band in the former case and the character and the orbital composition of the new band in the gap in the latter case would determine the normal and superconducting (if any exist) properties of alkali-metal doped solid cubane. For example, it is important to know whether the first conduction band remains flat by keeping its original orbital identity, and hence $\mathcal{D}(E_F)$ remains high, or whether it mixes strongly with the valence state of the alkali-metal atom. In the case of formation of a new alkali-metal band in the band gap, a situation would arise whereby a metallic lattice is incorporated into an insulating crystal. Furthermore, this metal could undergo a metal-insulator transition owing to the relatively large alkali-metal–alkali-metal distance. Hence, alkali-metal doped solid cubane (if it could be realized) would be an interesting system that might present several unusual features.

We take the center of the rhombohedral unit cell of solid cubane as the most favorable position for the dopant atom. We then optimize the structure of this alkali-metal doped solid cubane (designated as AC_8H_8 where A=Li, Na, or K) and determine the lattice parameters within the constraint of rhombohedral symmetry. Table I shows the optimized values of the rhombohedral lattice parameters and the corresponding changes in the unit cell volume for AC_8H_8 (A=Li, Na, or K). For all cases, the volume change is very large. We did not observe significant changes in the orientation of the cubane molecule with doping. We also observed that the Cartesian components of the stress tensor at the optimized structures were small (around 0.1–0.3 GPa) but not zero. This indicates that the rhombohedral symmetry can be lowered

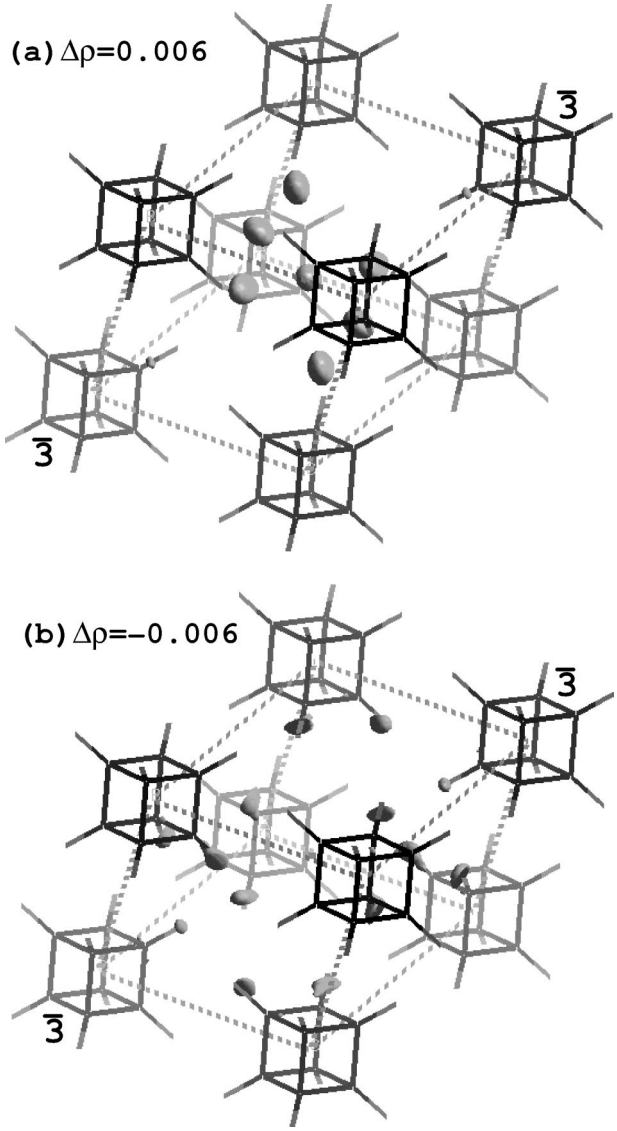

FIG. 9. Charge density difference isosurface [i.e., $\Delta\rho(\mathbf{r}) = \rho_{KC_8H_8} - \rho_{e-C_{8H_8}} - \rho_{K_R}$] for $\Delta\rho = 0.006$ (a) and -0.006 (b).

slightly upon releasing the symmetry constraint during the optimization.

In order to reveal the effect of the alkali-metal doping we calculated the electronic structure and charge densities of potassium doped cubane (KC_8H_8), the expanded cubane subsystem (e-C_8H_8) (where the K atoms are removed from KC_8H_8), and also the potassium subsystem (K_R or K only) (where cubane molecules in the KC_8H_8 structure are removed). In these calculations we used the same method and parameters as in the previous section. The $3s$ and $3p$ states are also considered as valence states in the pseudopotential of the potassium atom. Our results for the band structure and for the density of electronic states of K_R, e-C_8H_8, and KC_8H_8 are presented in Fig. 7. For the sake of better comparison, the energies of the lowest valence band derived from the molecular a_{1g} state of C_8H_8 and KC_8H_8 are aligned. Furthermore, the bands of K_R are shifted so that its Fermi level coincides with that of KC_8H_8. The form of the bands of solid cubane discussed in the previous section is slightly changed in e-C_8H_8. Furthermore, the valence bands of e-C_8H_8 are slightly modified upon K doping. Interestingly,

the lowest valence band of e-C_8H_8 derived from the valence orbital state a_{1g} of the cubane molecule occurs very near the K $3p$ states giving rise to a sharp peak. The first conduction bands of e-C_8H_8 and KC_8H_8 display similar forms and band widths ($\Delta E_W \sim 1$ eV), whereas the width of the first conduction band of K_R ($\Delta E_W \simeq 2$ eV) is larger than that of KC_8H_8. Upon K doping the first conduction band of e-C_8H_8 becomes detached from the rest of the conduction band by shifting downward by 0.5 eV, while its width is practically unaltered. This situation is also evident in the modification of the total density of states at the bottom of the conduction band in Fig. 7(d). In view of these facts, one can argue that the half-filled first conduction band of KC_8H_8 is derived mainly from the first conduction (LUMO) band of the solid cubane.

The character of the half-filled, first conduction band of KC_8H_8 and the contribution of K orbital states are further clarified by analysis of the state charge densities. In Fig. 8, we show the charge densities associated with the first conduction bands of K_R, e-C_8H_8, and KC_8H_8. It is seen that the charge density of K_R is not similar to that of KC_8H_8, in agreement with the discussion above; this excludes the possibility that the lowest conduction band of K doped solid cubane is not totally due to the dopant potassium. On the other hand, the charge density of KC_8H_8 displays some similarity to that of e-C_8H_8. Moreover, the isosurfaces of the charge density difference obtained from the charge densities presented in Fig. 8, i.e., $\Delta\rho = \rho_{KC_8H_8} - \rho_{C_8H_8} - \rho_{K_R}$, show significant charge rearrangements related to K as displayed in Fig. 9. We note that, while from the two cubane molecules along the threefold axis (labeled $\overline{3}$) there is no charge transfer, there is excess charge from the hydrogen atoms of the other six molecules pointing toward the K ion. Figure 9(b) shows negative charge density, which indicates that some of the electrons are pushed outward from the C-H bonds. These results suggest that the metallic band formed upon K doping is derived from the first conduction band of solid cubane with significant K $4s$ contribution. This band has low dispersion and hence has a high density of electronic states at the Fermi surface. It will be interesting to see if the conduction electrons in this band will couple with the high-energy intramolecular phonons of cubane to exhibit superconductivity.

VII. CONCLUSION

In this paper we investigated the C_8H_8 molecule, solid cubane, and alkali-metal doped cubane. We performed *ab initio* calculations to optimize the atomic structure and lattice parameters. Using the optimized structure, we calculated the electronic band structure, state densities, and charge density contour plots. We may summarize the important results as follows. (i) The electronic structure of the C_8H_8 molecule calculated within the local density approximation by using a plane wave basis set in periodically repeating supercell geometry and norm-conserving pseudopotentials is in good agreement with the level structure obtained with a local basis set. The normal modes calculated with a plane wave basis set can also reproduce all the features (both intensities and energies) obtained from the neutron inelastic scattering spectrum. (ii) Short-range chemical interactions play a dominant role in the cohesion of solid cubane. We found a cohesive energy per C_8H_8 molecule (due to the short-range interactions) of 0.68 eV for the fully optimized structure in the low-temperature, orientationally ordered phase. This corresponds to the global minimum of the rhombohedral structure. This value is significant for a molecular solid and explains why solid cubane is stable at room temperature. Significant energy lowering is achieved by optimization of the setting angle ϕ. (iii) The high-temperature, orientationally disordered phase corresponds to a local minimum. It occurs ~ 50 meV above the global minimum at $\alpha = 101.9°$. However, the energy of the system is rather insensitive to the setting angle in the range $25° < \phi < 95°$; this explains why the structure becomes orientationally disordered. (iv) The molecular orbitals of C_8H_8 dominate the band structure of solid cubane, in which the orbitals broaden into narrow bands. The locations of the peaks in the total density of states correlate very well with the level structure of the cubane molecule. We calculated a band gap between the valence (HOMO) and conduction (LUMO) bands of ~ 5 eV, which may be a slight underestimate. (v) Upon doping cubane with K, the lowest conduction band of solid cubane is slightly lowered and becomes half occupied. Our analysis of the relevant bands and their charge densities indicates that the metallic band of doped cubane is derived from undoped solid cubane's lowest conduction band with a significant contribution from the potassium atom.

ACKNOWLEDGMENTS

This work was supported in part by the National Science Foundation under Grant No. NSF-INT97-31014 and TÜBİTAK under Grant No. TBAG-1668(197 T 116).

*Present address: Department of Physics and Astronomy, The University of North Carolina at Chapel Hill, Chapel Hill, NC 27599.

[1] P.E. Eaton and T.W. Cole, Jr., J. Am. Chem. Soc. **86**, 962 (1964).
[2] P.E. Eaton, Angew. Chem. **31**, 1421 (1992).
[3] B.D. Kybett, S. Carroll, P. Natollis, D.W. Bonnell, J.L. Margrave, and J.L. Franklin, J. Am. Chem. Soc. **88**, 626 (1966).
[4] S. Borman, Chem. Sci. Eng. News **72**, 34 (1994).
[5] T.W. Cole, J. Perkins, S. Putnam, P.W. Pakes, and H.L. Straus, J. Phys. Chem. **85**, 2185 (1981).
[6] R.A. Dalterio and F.J. Owens, Solid State Commun. **67**, 673 (1988).
[7] E.W. Della, E.F. McCoy, H.K. Patney, G.L. Jones, and F.A. Miller, J. Am. Chem. Soc. **101**, 7441 (1979).
[8] A.S. Pine, A.G. Maki, A.G. Robiette, B.J. Krohn, J.K.G. Watson, and Th. Urbanek, J. Am. Chem. Soc. **106**, 891 (1984).
[9] E.B. Fleischer, J. Am. Chem. Soc. **86**, 3889 (1964).
[10] J.M. Schulman, C.R. Fischer, P. Solomon, and T.J. Venanzi, J. Am. Chem. Soc. **100**, 2949 (1978).
[11] W. Scamehorn, M. Yoshimine, and J. Pacansky, J. Phys. Chem. **85**, 1340 (1981).
[12] J. Almlof and T. Jonvik, Chem. Phys. Lett. **92**, 267 (1982).
[13] C.A. Scamehorn, S.M. Hermiller, and R.M. Pitzar, J. Chem. Phys. **84**, 833 (1986).
[14] T. Yildirim, Ç. Kılıç, S. Ciraci, P.M. Gehring, D.A. Neumann,

P.E. Eaton, and T. Emrick, Chem. Phys. Lett. **309**, 234 (1999).
[15] Ç. Kılıç, T. Yildirim, H. Mehrez, and S. Ciraci, J. Phys. Chem. **104**, 2724 (2000).
[16] V. Glasso, Chem. Phys. **184**, 107 (1994).
[17] P.M. Gehring, D.A. Neumann, W.A. Kamitakahara, J.J. Rush, P.E. Eaton, and D.P. VanMeurs, J. Phys. Chem. **99**, 4429 (1995).
[18] M.A. White, R.E. Wasylishen, P.E. Eaton, Y. Xiong, K. Pramod, and N. Nodari, J. Phys. Chem. **96**, 421 (1992).
[19] A. Detken, H. Zimmermann, U. Haeberlen, R. Poupko, and Z. Luz, J. Phys. Chem. **100**, 9598 (1996).
[20] T. Yildirim, P.M. Gehring, D.A. Neumann, P.E. Eaton, and T. Emrick, Phys. Rev. Lett. **78**, 4938 (1997).
[21] T. Yildirim, P.M. Gehring, D.A. Neumann, P.E. Eaton, and T. Emrick, Phys. Rev. B **60**, 314 (1999).
[22] T. Yildirim, P.M. Gehring, D.A. Neumann, P.E. Eaton, and T. Emrick, Carbon **36**, 809 (1997).
[23] T. Yildirim, A. Buldum, S. Ciraci, and C.Y. Fong, Bull. Am. Phys. Soc. **43**(1), 25 (1998).
[24] S.L. Richardson and J.L. Martins, Phys. Rev. B **58**, 15 307 (1998).
[25] K.H. Mitchel and K. Parlinski, Phys. Rev. B **31**, 1823 (1985); M. Yvinec and R.M. Pick, J. Phys. (Paris) **41**, 1045 (1980).
[26] L. Kleinman and D.M. Bylander, Phys. Rev. Lett. **48**, 1425 (1982).
[27] D.M. Ceperley and B.J. Alder, Phys. Rev. Lett. **45**, 556 (1980).
[28] J.P. Perdew and A. Zunger, Phys. Rev. B **23**, 5048 (1981).
[29] Identification of commercial products does not imply recommendation or endorsement by the National Institute of Standards and Technology.
[30] M.C. Payne, M.P. Teter, D.C. Allen, T.A. Arias, and J.D. Joannopoulos, Rev. Mod. Phys. **64**, 1045 (1992). The computer code CASTEP is distributed and maintained by Molecular Simulations Inc.
[31] H. Monkhorst and J.D. Pack, Phys. Rev. B **13**, 5188 (1976).
[32] W.H. Press *et al.*, *Numerical Recipes* (Cambridge University Press, Cambridge, 1989).
[33] M. J. Frisch *et al.*, GAUSSIAN 94, Gaussian, Inc., Pittsburg, PA, 1995.
[34] L. Hedberg, K. Hedberg, P.E. Eaton, N. Nodari, and A.G. Robiette, J. Am. Chem. Soc. **113**, 1514 (1991).
[35] A.D. Becke, J. Chem. Phys. **98**, 5648 (1993).
[36] S. Lovesay, *Theory of Neutron Scattering from Condensed Matter*, 3rd ed. (Oxford University Press, New York, 1987).
[37] E.M. Lifshitz, Zh. Exp. Teor. Fiz. **29**, 94 (1956) [Sov. Phys. JETP **2**, 73 (1956)].
[38] J. N. Israelachvili, *Intermolecular and Surface Forces* (Academic, London, 1985).
[39] J.E. Inglesfield and E. Wikborg, J. Phys. F: Met. Phys. **5**, 1475 (1975); J.E. Inglesfield, *ibid.* **6**, 687 (1976).
[40] S. Ciraci, E. Tekman, A. Baratoff, and I.P. Batra, Phys. Rev. B **46**, 10 411 (1992).
[41] R. Pérez, I. Stich, M.C. Payne, and K. Terakura, Phys. Rev. B **58**, 10 835 (1998).
[42] T. Yildirim, Chem. Phys. Special Issue on *Condensed Phase Structure and Dynamics: A Combined Neutron Scattering and Numeric Modelling Approach* (2000).
[43] N.D. Lang, Phys. Rev. Lett. **46**, 342 (1981).
[44] S. Ishi and B. Viswanathan, Thin Solid Films **201**, 373 (1991).
[45] A. Baratoff, S. Ciraci, and E. Stoll (unpublished).
[46] T.A. Halgren, J. Am. Chem. Soc. **114**, 7827 (1992).
[47] P. Vinet, J.H. Rose, J. Ferrante, and J.R. Smith, J. Phys.: Condens. Matter **1**, 1941 (1989).
[48] J.L. Martins and N. Troullier, Phys. Rev. B **46**, 1766 (1992).
[49] N. Troullier and J.L. Martins, Solid State Commun. **74**, 613 (1990); Phys. Rev. B **43**, 1993 (1991).